Available online at www.sciencedirect.com
SCIENCE DIRECT®
Inorganica Chimica Acta 353 (2003) 253–262
Inorganica Chimica Acta
www.elsevier.com/locate/ica

Reaction of copper(II) with 1-carboxamide-3,5-dimethylpyrazole, 1-carboxamidine-3,5-dimethylpyrazole, 4-acetyl-3-amino-5-methylpyrazole and 5-amino-4-carboxamide-1-phenylpyrazole☆

K. Mészáros Szécsényi [a,*], V.M. Leovac [a], V.I. Češljević [a], A. Kovács [b], G. Pokol [c], Gy. Argay [d], A. Kálmán [d], G.A. Bogdanović [e], Ž.K. Jaćimović [f], A. Spasojević-de Biré [g]

[a] Department of Chemistry, University of Novi Sad, Faculty of Sciences, 21000 Novi Sad, Trg D. Obradovića 3, Serbia and Montenegro
[b] Research Group of Technical Analytical Chemistry of the Hungarian Academy of Sciences at the Institute of General and Analytical Chemistry, Budapest University of Technology and Economics, H-1521 Budapest, Hungary
[c] Institute of General and Analytical Chemistry, Budapest University of Technology and Economics, H-1521 Budapest, Hungary
[d] Institute of Chemistry, Chemical Research Center, Hungarian Academy of Sciences, P.O. Box 17, H-1525 Budapest, Hungary
[e] Laboratory of Theoretical Physics and Condensed Matter Physics, VINČA Institute of Nuclear Sciences, P.O. Box 522, 11001 Belgrade, Serbia and Montenegro
[f] Faculty of Metallurgy and Technology, University of Montenegro Podgorica, Serbia and Montenegro
[g] Laboratoire de Structures, Properiétés et Modélisation des Solides (SPMS), UMR 8580 du CNRS, Ecole Centrale Paris, Grande Voie des Vignes, 92295 Chaatenay-Malabry Cedex, France

Received 19 December 2002; accepted 28 February 2003

Abstract

Complex formation of copper(II) bromide and acetate with 1-carboxamide-3,5-dimethylpyrazole (HL^3) and copper(II) bromide with 5-amino-4-carboxamide-1-phenylpyrazole (L^2), 4-acetyl-3-amino-5-methylpyrazole (HL^4) and 1-carboxamidine-3,5-dimethylpyrazole (HL^5), was studied. The obtained compounds, $\mathbf{CuBr_2(L^2)_2}$, $\mathbf{Cu(L^3)_2}$, $\mathbf{CuBr_2(HL^4)_2}$, $\mathbf{CuBr_2(HL^5)_2}$ and $\mathbf{[CuBr(HL^1)(L^3)]_2}$ (HL^1 denotes the 3,5-dimethylpyrazole), are characterized by elemental analysis, FT-IR spectrometry, molar conductivity, TG-MS and DSC. The X-ray structure of $[CuBr(HL^1)(L^3)]_2$ and $Cu(L^3)_2$ is discussed. For $\mathbf{[CuBr(HL^1)(L^3)]_2}$ a dimeric penta-co-ordinated structure has been found; the co-ordination around the metal in $\mathbf{Cu(L^3)_2}$ is *trans*-square planar. To $\mathbf{CuBr_2(L^2)_2}$ and $\mathbf{CuBr_2(HL^4)_2}$ a nearly tetrahedral, while for $\mathbf{CuBr_2(HL^5)_2}$ an octahedral geometry may be assumed. It means that the geometry of the compounds in the first place depends on the ligand substituents. The course of the complex formation reaction is anion-dependent and may be explained on the basis of Pearson's theory, taking into account the steric factors. A low stability intermediate formation was observed in the thermal decomposition of $\mathbf{Cu(L^3)_2}$.

Keywords: Pyrazole-complexes; Copper(II)-complexes; Pearson theory

1. Introduction

Complexes with pyrazole-based ligands are a frequent subject of chemical investigations giving an opportunity for a better understanding the relationship between the structure and the activity of the active site of metalloproteins. Namely, the metal ion in biological systems is often co-ordinated to one or more imidazole groups which are part of histidine fragments of the proteins [2]. On the other hand, the aromatic ring systems of imidazoles and pyrazoles are very much alike in the electronic and steric sense, but the latter ones more readily synthesized compared to the former ligands. Hence, there are excellent review articles on the pyrazole-based co-ordination compounds [3–5]. Nowadays, attention is paid to the design of various pyrazole ligands with special structural properties to fulfill the

☆ This paper is Part 14 in the series of our studies on Transition Metal Complexes with pyrazole-based ligands. Part 13 [1].

* Corresponding author. Tel.: +381-21-35-0122x832; fax: +381-21-54-065.
E-mail address: mszk@eunet.yu (K. Mészáros Szécsényi).

0020-1693/03/$ - see front matter © 2003 Elsevier B.V. All rights reserved.
doi:10.1016/S0020-1693(03)00231-7

specific stereochemical requirements of a particular metal-binding site [6]. The review [6] deals with the co-ordination chemistry of transition metal complexes with bi- and polydentate pyrazole derivatives.

In our systematic studies on transition metal complexes the pyrazole derivatives take part in co-ordination mostly as monodentate ligands [7–9]. However, during thermal treatment of the compounds, depending on the pyrazole substituents, relatively stable intermediates with a stoichiometric composition are formed, whereby the co-ordination mode of the ligand changes. This points to a possibility of a solid phase synthesis of new compounds. The goal of our systematic studies on pyrazole complexes with transition metal ions is to examine how the substituents of the pyrazole ring, as well as various cations and anions, influence the course of the complex formation reaction. Additionally, our aim is to gain information on the structural dependence of the thermal properties within the investigated series.

In this part we report the synthesis, physico-chemical characteristics and structure of copper(II) complexes formed with 5-amino-4-carboxamide-1-phenylpyrazole, (L^2), 1-carboxamide-3,5-dimethylpyrazole, (HL^3), 4-acetyl-3-amino-5-methylpyrazole (HL^4) and 1-carboxamidine-3,5-dimethylpyrazole, (HL^5) ligands. Compounds with the following compositions are obtained: **$CuBr_2(L^2)_2$**, **$Cu(L^3)_2$**, **$CuBr_2(HL^4)_2$**, **$CuBr_2(HL^5)_2$** and **$[CuBr(HL^1)(L^3)]_2$**, where HL^1 denotes the 3,5-dimethylpyrazole ligand.

2. Experimental

2.1. General procedures

All pyrazole derivatives were reagent grade, commercial products of Aldrich Company, except of HL^4. Its synthesis was described previously [10]. The copper(II) salts were analytical reagent grade. The IR-spectra were recorded in the range of 4000–150 cm^{-1} on a Perkin–Elmer System 2000 FT-IR spectrometer at room temperature using KBr pellets in the mid-IR range and polyethylene pellets in the far-IR range. The spectra were obtained with a resolution of 4 cm^{-1} and with a co-addition of 16 scans. The thermal analysis was carried out using a DuPont 2000 TA system with a thermobalance DuPont 951 TGA. At the thermogravimetric measurements the samples were heated in a platinum crucible with a heating rate of 10 K min^{-1} up to 1000 K. With the same heating rate the DSC curves were registered up to 600 K using an open aluminium pan as sample holder and an empty aluminium pan as reference. For the TG-MS measurements a TA Instruments SDT 2960 was employed, coupled with Balzers Termostar GSD 300 T capillary MS. The molar conductivity of freshly prepared 10^{-3} mol dm^{-3} solutions of the compounds in DMF was measured at room temperature using a Jenway 4010 conductivity meter. Magnetic susceptibility measurements were conducted at room temperature by means of a magnetic susceptibility balance MSB-MKI, Sherwood Scientific Ltd, Cambridge. The data were corrected for diamagnetic susceptibilities.

2.2. Synthesis

All the compounds were synthesized by mixing warm ethanolic solutions of the ligand (2 mmol) and copper(II) bromide (1 mmol) except for $Cu(L^3)_2$, where copper(II) acetate monohydrate was used instead, and both the ligand (2 mmol) and the metal salt (1 mmol) were dissolved in methanol. The total volume of the mixture was about 10 cm^3. The coloured precipitates were obtained at room temperature. The formed compounds were washed with cold EtOH and Et_2O and dried at room temperature.

2.2.1. $[CuBr(HL^1)(L^3)]_2$

Reaction time: 24 h. Colour: green. Yield: 64.7%. μ_{eff}, μ_B: 1.72. λ_M, S cm^2 mol^{-1}: 31.5. Elemental analysis data (Found (Required)%): C, 33.10 (34.98); H, 3.94 (4.27); N, 18.80 (18.54).

2.2.2. $CuBr_2(L^2)_2$

Reaction time: 0.5 h. Colour: black. Yield: 74.2%. μ_{eff}, μ_B: 2.19. λ_M, S cm^2 mol^{-1}: 55.0. Elemental analysis data (Found (Required)%): C, 38.60 (38.26); H, 3.78 (3.21); N, 18.22 (17.85).

2.2.3. $Cu(L^3)_2$

Reaction time: 3 h. Colour: blue. Yield: 76.5%. μ_{eff}, μ_B: 1.80. λ_M, S cm^2 mol^{-1}: 14.6. Elemental analysis data (Found (Required)%): C, 42.62 (42.40); H, 5.21 (4.75); N, 24.50 (24.73).

2.2.4. $CuBr_2(HL^4)_2$

Reaction time: 15 h. Colour: black. Yield: 83.3%. μ_{eff}, μ_B: 1.85. λ_M, S cm^2 mol^{-1}: 48.4. Elemental analysis data (Found (Required)%): C, 28.67 (28.73); H, 3.77 (3. 62); N, 16.90 (16.75).

2.2.5. $CuBr_2(HL^4)_2$

Reaction time: 24 h. Colour: blue. Yield: 75.0%. μ_{eff}, μ_B: 1.83. λ_M, S cm^2 mol^{-1}: 95.1. Elemental analysis data (Found (Required)%): C, 29.31 (28.84); H, 3.79 (4.03); N, 23.38 (22.73).

All the compounds were characterized by FT-IR spectrometry. Compounds **$[CuBr(HL^1)(L^3)]_2$** and **$Cu(L^3)_2$** were also studied by single crystal X-ray structure analysis. The structure of the compounds is presented in ORTEP projection [11]. For the compounds

Table 1
IR assignments

$CuBr_2(L^2)$	$CuBr_2(HL^4)_2$	$CuBr_2(HL^5)_2$	Assignment
	3439 s	3312 s	NH stretch
	3305 s [a]		NH stretch
3427 s	3146 s	3262 sh	NH_2 asymmetric stretch
	2962 m [a]		NH_2 asymmetric stretch
3341 s	3050 s	3104 s	NH_2 symmetric stretch
	2852 m [a]		NH_2 symmetric stretch
3090 vw			aryl CH stretch
3067 vw			aryl CH stretch
3050 vw			aryl CH stretch
2967 vw			CH_3 asymmetric stretch
2931 vw		2924 vw	CH_3 symmetric stretch
		1665 vs	imine C=N stretch
1648 vs	1623 vs		CO stretch
1625 vs			pyr skeleton stretch+CN stretch
1610 sh			aryl skeleton stretch
1596 sh	1563 w	1591 m	pyr skeleton stretch (+NH_2 scissoring) [b]
1587 sh			aryl skeleton stretch
1552 s	1536 s	1565 m	pyr skeleton stretch (+NH_2 scissoring) [b]
1516 w			aryl skeleton stretch
1497 m	1480 s	1494 s	CH_3 asymmetric def+pyr skeleton stretch
		1468 m	CH_3 asymmetric def
1458 m			aryl skeleton stretch
1441 s	1450 m	1448 w	CH_3 asymmetric def
	1414 w	1411 s	CH_3 asymmetric def+pyr skeleton stretch
	1386 m	1384 m	CH_3 symmetric def+pyr skeleton stretch
	1372 sh	1373 sh	CH_3 symmetric def+pyr skeleton stretch
1353 m		1356 s	CH_3 symmetric def
	1320 s		NH bend+pyr skeleton stretch
1315 w	1310 sh	1312 m	pyr skeleton stretch+def
		1249 m	C–N stretch
1296 m			aryl in-plane CH bend
1287 m			aryl in-plane CH bend
1230 m			aryl in-plane CH bend
1175 w			aryl in-plane CH bend
1131 w	1147 m	1134 m	pyr skeleton stretch
1092 w	1095 m	1078 w	CC stretch+pyr skeleton def
1077 w	1071 w	1058 m	NH_2 rock+pyr skeleton stretch
1046 w	1037 w	1030 w	CH_3 rock
1019 w	1025 w		pyr skeleton stretch+NH_2 rock
962 m	960 m	994 m	CC stretch+CH_3 rock
916 m			aryl CH wag
		843 m	imine NH wag
	801 m	806 w	pyr skeleton def+CN stretch
777 m			aryl CH wag
754 m	742 m	769 m	C–NH_2 bend+pyr skeleton torsion
734 m			aryl skeleton bend
697 m			aryl CH wag
		714 w	NCN bend
664 w	680 m	665 w	CC stretch+C–CH_3 bend
631 w		648 w	pyr skeleton torsion
591 w	592 m		CO wag+CH_3 rock
	583 sh		pyr skeleton def+CC stretch
	562 w	582 w	NH_2 torsion+NH_2 wag
537 w			aryl ring torsion
500 m	451 s	516 s	NH_2 wag +NH_2 torsion
	470 s		NH wag+C–CH_3 wag
423 w	367 w	408 w	Cu–Br stretch
369 w	323 m	343 m	pyr skeleton torsion
		313 w	C–CH_3 wag+C–NH_2 wag
251 w	245 w	285 w	Cu–N stretch
212 w		210 w	CH_3 torsion

[a] Observed also in the IR spectrum of the ligand [12]; may be attributed to different pattern of intermolecular interactions in the crystal.
[b] NH_2 scissoring may contribute to these fundamentals in derivatives with an NH_2 group.

with no X-ray data the IR assignments [12–14] are given in Table 1.

2.3. Crystal structure determination

Crystal data for **[CuBr(HL^1)(L^3)]$_2$** and **Cu(L^3)$_2$** were collected at room temperature on Enraf-Nonius CAD-4 diffractometers [15] in different laboratories (Paris, Budapest), using Mo Kα radiation ($\lambda = 0.71073$ Å) and $\omega/2\theta$ scans. Data correction [16] and absorption correction was applied: psi-scan type [17] for **Cu(L^3)$_2$** and Gaussian-type [18], based on the crystal morphology ($T_{min} = 0.335$, $T_{max} = 0.735$) for **[CuBr(HL^1)(L^3)]$_2$**.

The structures were solved by heavy atom [19] and difference Fourier methods and refined on F^2 by full-matrix least-squares method [20]. The weighting schemes were $w = 1/[\sigma^2(F_o^2)+(0.1731P)^2]$ and $w = 1/[\sigma^2(F_o^2)+(0.1000P)^2]$ for **[CuBr(HL^1)(L^3)]$_2$** and **Cu(L^3)$_2$**, respectively; $P = (F_o^2+2F_c^2)/3$. In both crystal structures non-hydrogen atoms were refined with anisotropic displacement parameters. In refinement of **Cu(L^3)$_2$** some least-squares restraints (ISOR, DELU for all non-hydrogen atoms, DFIX and SADI for N–H distances) were used. H atoms (except H7 and H17 in Cu(L^3)$_2$, they were located in difference map) were placed in calculated positions and refined with isotropic displacement parameters. In the case of **[CuBr(HL^1)(L^3)]$_2$** all H atoms were placed in calculated positions (for the purpose of decreasing the number of refined parameters) and they are in good agreement with positions located in difference maps. Details and final R values are given in Table 2, together with other experimental data relevant to the X-ray analyses. Note: unit cell dimensions for **[CuBr(HL^1)(L^3)]$_2$** can be transformed to the next values: $a = 8.965$ Å, $b = 9.277$ Å, $c = 10.734$ Å, $\alpha = 73.47°$, $\beta = 71.67°$, $\gamma = 61.18°$.

Table 2
Crystal data and structure refinement for **[CuBr(HL^1)(L^3)]$_2$** and **Cu(L^3)$_2$**

	[CuBr(HL^1)(L^3)]$_2$	Cu(L^3)$_2$
Empirical formula	$C_{22}H_{32}Br_2Cu_2N_{10}O_2$	$C_{12}H_{16}CuN_6O_2$
Formula mass	755.5	339.85
Temperature (K)	293(2)	293(2)
Wavelength (Å)	0.710730	0.710730
Crystal system	triclinic	triclinic
Space group	$P\bar{1}$	$P\bar{1}$
Unit cell dimensions		
a (Å)	9.277(4)	8.461(1)
b (Å)	9.287(5)	8.631(1)
c (Å)	10.734(5)	10.745(2)
α (°)	91.11(4)	68.72(1)
β (°)	106.53(4)	70.29(1)
γ (°)	122.25(4)	77.64(1)
Volume (Å^3)	732.9(6)	684.57(17)
Z	1	2
Density (calculated) (Mg m^{-3})	1.712	1.649
Absorption coefficient (mm^{-1})	4.215	1.610
F(0 0 0)	378	350
Crystal size (mm)	0.25 × 0.21 × 0.08	0.50 × 0.25 × 0.20
θ range for data collection (°)	$2.02 \le \theta \le 27.99$	$2.55 \le \theta \le 38.47$
Index ranges	$-12 \le h \le 11$; $-12 \le k \le 12$; $0 \le l \le 14$	$-14 \le h \le 13$; $-15 \le k \le 14$; $-18 \le l \le 8$
Reflections collected	3723	8193
Independent reflections	3533 [$R_{int} = 0.0235$]	7666 [$R_{int} = 0.0137$]
Refinement method	Full-matrix least-squares on F^2	Full-matrix least-squares on F^2
Data/restraints/parameters	3533/0/172	7666/193/196
Goodness-of-fit on F^2	1.031	0.907
Final R indices [$I > 2\sigma(I)$]	$R_1 = 0.0869$, $wR_2 = 0.2247$	$R_1 = 0.0449$, $wR_2 = 0.1315$

3. Results and discussion

The complexes are coloured and stable in air. They are soluble in DMF and MeOH, slightly soluble in EtOH, but insoluble in H_2O and Et_2O. The molar conductivity for all of the compounds was measured in DMF. A low molar conductivity is characteristic for the **Cu(L^3)$_2$** referring to its non-electrolytic character, while in the case of the **CuBr$_2$(HL^5)$_2$** the value of the molar conductivity corresponds to an electrolyte of 1:1 type [21]. The molar conductivity of the other complexes suggests only a partial replacement of the bromide ion by the solvent molecule:

$$CuBr_2(L)_2 + DMF \rightleftharpoons CuBr(L)_2DMF^+ + Br^-$$

where (L) denotes (L^2) and (HL^4). The same is valid for the **[CuBr(HL^1)(L^3)]$_2$** complex with mixed ligands. Nonetheless, for these compounds the co-ordination of the anion may be regarded as non-ionic, even in solution.

3.1. Description of the structures

3.1.1. [CuBr(HL^1)(L^3)]$_2$

The compound has a dimeric centrosymmetric structure (Fig. 1) with a Cu···Cu′ distance of 3.72 Å. The co-ordination around the Cu atom is a square pyramid, formed by co-ordination of the N1 atom of the

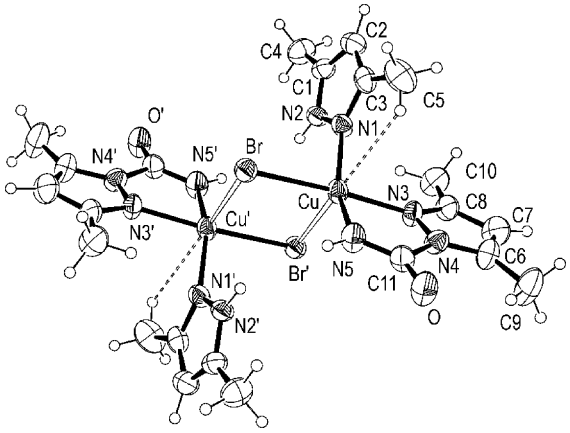

Fig. 1. ORTEP drawing of complex $[CuBr(HL^1)(L^3)]_2$ with atom numbering scheme.

monodentate HL^1 and N3 and N5 of the bidentate L^3 as well as the bridging bromine atoms—Br in the equatorial plane and Br′ in the apical position. As the ligand L^3 is approximately planar with C9–H···O, an intramolecular hydrogen-bond formation takes place, yielding a six-membered C9–H···O–C11–N4–C6 ring. The copper atoms are displaced from the equatorial N1–N3–N5–Br co-ordination plane to the apical Br′ atom for an expectable value of 0.24 Å. However, the arrangement of the atoms in the equatorial plane is quite irregular. Namely, the N3, N5 and Br atoms together with the two Cu atoms are almost ideally coplanar (root-mean-square deviation of N3, N5, Br, Cu atoms is 0.006 Å) what is an unusual position for a square-pyramidal co-ordination. This geometry may be explained by the interaction between the metal atom and the C5 methyl group's hydrogen that is supported by the short Cu···H distance (2.67 Å). Besides, the N1–C3–C5 angle is much smaller than the C2–C3–C5 one. It means that the C5 methyl group is shifted towards Cu. Although the rotation of HL^1 around the Cu–N1 bond is possible, it is oriented in such a way as to enable the Cu···H contact in the Cu–N1–C3–C5 plane with a torsion angle of nearly 0°. As a consequence, N1 is displaced from the N3–N5–Br–Cu plane for 0.82 Å (Fig. 2), because the whole HL^1 is shifted out of the equatorial plane to obtain the best position for the Cu···H interaction, resulting a pseudo-octahedral surrounding around the copper atom. The bridging Br′ and H(···Cu) atoms are displaced from the N1–N3–N5–Br equatorial plane for 2.98 and 2.24 Å, respectively, and to the opposite direction forming a Br′–Cu–H angle of 153°.

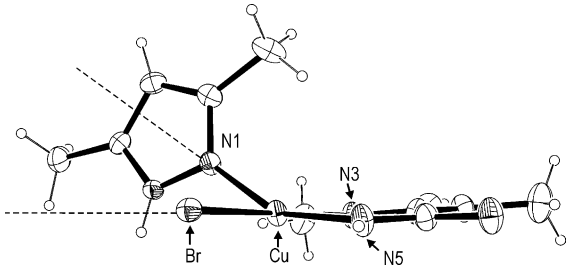

Fig. 2. The equatorial plane of complex $[CuBr(HL^1)(L^3)]_2$ with displaced position of N1 atom to the Br–Cu–N3–N5 plane.

The angle between the mean planes of the two pyrazole rings is 78°. There is a short $HL^1\cdots L^3$ interligand contact of 3.26 Å between the C10 methyl group and the N1 atom, enabling a short C–H···π interaction between a hydrogen atom of C10 and the N1–N2 bond centroid (Cg) with a H···Cg distance of about 2.6 Å.

In the crystal lattice, the binuclear molecules are mutually connected by intermolecular N2–H···O, N5–H···O and C4–H···O hydrogen bonds forming 3D supramolecular structure. The geometrical parameters of the H-bonds are: N2–H2N = 0.86Å, N2···O(i) = 3.16Å, H2N···O(i) = 2.43 Å, N2–H2N···O(i) = 172°; N5–H5N = 0.86 Å, N5···O(ii) = 3.01 Å, H5N···O(ii) = 2.16 Å, N5–H5N···O(ii) = 172°; C4–H4A = 0.96 Å, C4···O(i) = 3.24 Å, H4A···O(i) = 2.36 Å, C4–H4A···O(i) = 151°; symmetry code: (i) $x-1,+y-1,+z$; (ii) $-x+1,-y+1,-z$. The packing diagram for the compound is presented in Fig. 3, while the interatomic bond lengths and selected bond angles in the complex are given in Table 3.

3.1.2. $Cu(L^3)_2$

The α-modification of this compound was synthesized by Valach et al. [22] by the reaction of freshly obtained $[Cu(NCO)_2(2,4\text{-}Me_2py)]$ with 3,5-dimethylpyrazole ligand in a methanolic solution at 278 K. The crystal structure of this modification was determined by X-ray structure analysis. By similar method, at higher temperature the former authors obtained the β-modification of the same compound also, in form of blue flakes.

In our case, the compound was prepared by the reaction of copper(II) acetate with 1-carboxamide-3,5-

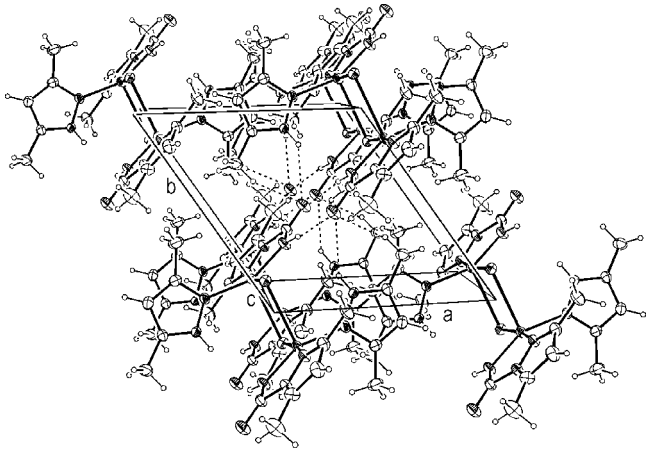

Fig. 3. Projection of the crystal packing along crystallographic '*c*' axis for $[CuBr(HL^1)(L^3)]_2$ (the dashed lines show the hydrogen bonds).

Table 3
Interatomic bond lengths (Å) and selected bond angles (°) for **[CuBr(HL^1)(L^3)]$_2$**

Bond lengths			
Cu–N5	1.909(8)	C3–C5	1.501(15)
Cu–N1	1.988(8)	N3–C8	1.328(12)
Cu–N3	2.019(8)	N3–N4	1.341(11)
Cu–Br	2.4786(19)	N4–C6	1.344(13)
Cu–Br′	2.770(2)	N4–C11	1.455(13)
N1–C3	1.342(12)	N5–C11	1.290(13)
N1–N2	1.357(10)	C6–C7	1.343(17)
N2–C1	1.318(12)	C6–C9	1.504(17)
C1–C2	1.370(14)	C7–C8	1.437(16)
C1–C4	1.503(15)	C8–C10	1.468(15)
C2–C3	1.392(15)	O–C11	1.246(12)
Bond angles			
N5–Cu–N1	154.3(4)	N5–Cu–Br′	110.5(3)
N5–Cu–N3	79.9(4)	N1–Cu–Br′	94.6(2)
N1–Cu–N3	93.9(3)	N3–Cu–Br′	93.6(3)
N5–Cu–Br	91.7(3)	Br–Cu–Br′	90.08(7)
N1–Cu–Br	93.4(2)	Cu–Br–Cu′	89.92(7)
N3–Cu–Br	171.5(2)		

dimethylpyrazole. By the deprotonation of the ligand the blue β-modification of Cu(L^3)$_2$ was obtained in a single crystalline form, suitable for an X-ray structure analysis. The deprotonation of the NH_2-group (leading to L^3 in the complex) is well reflected also by the IR spectrum of the complex, where the respective NH stretching band has vanished. Additional information provided by IR spectrometry is the unchanged position of the ν(C=O) vibrational band upon complex formation indicating that the oxygen atom is not involved in a coordinative bonding with Cu. The IR-spectral data are in accordance with the X-ray analysis. Namely, the oxygen atoms are not involved in co-ordination with the central atom because the Cu–O distances for the adjacent molecules are greater than 3.3 Å [23]. The co-ordination is established through the nitrogen atom of the deprotonated carboxamide group and the pyridine nitrogen atom from two ligand molecules.

Both crystalline modifications have a distorted *trans* square-planar arrangement around the central atom. The ORTEP drawing for the β-modification is presented in Fig. 4. The main difference between the two structures is that the α-modification belongs to monoclinic $P2_1/c$ space group with $Z=4$, while the β-modification to triclinic $P\bar{1}$ space group with $Z=2$. The interatomic distances and bond angles are given in Table 4 for both α- and β-modifications. The differences are not significant.

In the crystal lattice of the β-modification molecules form N7–H7···O8(iii) dimers (Fig. 5), with the following geometrical parameters: N7–H7 = 0.78 Å, N7···O8(iii) = 3.206(2) Å, H7···O8(iii) = 2.43 Å, N7–H7···O8(iii) = 176.7°; symmetry code (iii) $-x, -y+1, -z$.

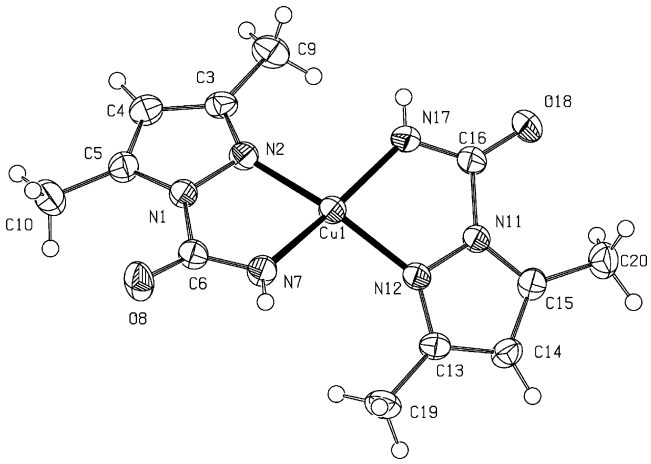

Fig. 4. ORTEP drawing of complex Cu(L^3)$_2$ with atom numbering scheme.

The magnetic moment of the **Cu(L^3)$_2$** and **[CuBr(HL^1)(L^3)]$_2$** complexes ($\mu_{eff}=1.80$ and 1.72 μ_B, respectively) is characteristic for the $S=1/2$ systems. The lower μ_{eff} value for **[CuBr(HL^1)(L^3)]$_2$** is in agreement with its bridged structure.

In complexes with L^2 and HL^4, **Cu(L^2)$_2$Br$_2$** and **Cu(HL^4)$_2$Br$_2$**, the pyrazole derivative acts as monodentate ligand through the pyridine ring nitrogen atom. In principle, most of the copper(II) complexes should have a tetrahedral geometry with a magnetic susceptibility of about 2.2 [24]. On this basis ($\mu_{eff}=2.19$) for the **Cu(L^2)$_2$Br$_2$** complex a tetrahedral geometry may be assumed, also. For the bis(ligand) complexes of $CuCl_2$ with HL^4 a distorted tetrahedral geometry was found by X-ray analysis [10]. As the space requirement of the bromine atoms is larger, for the bromide complex, **Cu(HL^4)$_2$Br$_2$**, with the same ligand, a tetrahedral geometry may be proposed.

Copper(II) bromide with HL^5 also forms a bis(ligand) complex. Its structure seems to have similar geometry as the analogous copper(II) nitrate complex whose structure was determined by X-ray analysis [25]. In this compound the copper(II) is co-ordinated endobidentate to the pyridine-type and the =NH nitrogen atoms of the ring and the carboxamidine group, respectively. The nitrate groups are bonded as monodentate species in the axial positions providing thus an octahedral environment around the metal atom. As the complexing ability of the nitrate is low, it is not co-ordinated in solution. Bromides form more readily complexes than nitrates. However, the molar conductivity of the corresponding bromide complex is also high and corresponds to an 1:1 electrolyte. Based on this, for the **CuBr$_2$(HL^5)$_2$** a similar octahedral geometry could be proposed.

Table 4
Interatomic bond lengths (Å) and selected bond angles (°) for β-**Cu(L^3)$_2$** compared to those found in α-modification [22]

Bond lengths	β	α	Bond lengths	β	α
Cu1–N2	1.999(1)	1.985(8)	Cu1–N12	1.996(1)	1.990(8)
Cu1–N7	1.924(1)	1.926(8)	Cu1–N17	1.924(2)	1.908(10)
N1–N2	1.372(2)	1.363(11)	N11–N12	1.367(2)	1.363(11)
N1–C5	1.356(2)	1.345(13)	N11–C15	1.357(2)	1.368(13)
N2–C3	1.328(2)	1.352(11)	N12–C13	1.335(2)	1.316(12)
C3–C4	1.405(3)	1.370(16)	C13–C14	1.409(2)	1.367(15)
C4–C5	1.376(2)	1.388(14)	C14–C15	1.379(2)	1.358(13)
C3–C9	1.494(2)	1.461(14)	C13–C19	1.494(2)	1.493(14)
C5–C10	1.488(2)	1.487(15)	C15–C20	1.484(2)	1.481(16)
N1–C6	1.450(2)	1.465(11)	N11–C16	1.450(2)	1.432(12)
C6–N7	1.315(2)	1.313(14)	C16–N17	1.311(2)	1.306(16)
C6–O8	1.228(2)	1.220(13)	C16–O18	1.229(2)	1.218(14)
N2–Cu1–N7	81.98(6)	81.5(3)	N12–Cu1–N17	81.16(6)	81.0(3)
N2–Cu1–N17	100.66(6)	99.8(3)	N12–Cu1–N17	102.46(6)	99.0(3)
N2–Cu1–N12	157.21(6)	173.5(3)	N7–Cu1–N17	164.32(8)	168.9(3)
N1–N2–Cu1	109.78(9)	111.0(5)	N11–N12–Cu1	110.6(1)	110.4(5)
C3–N2–Cu1	141.9(1)	143.1(6)	C13–N12–Cu1	142.4(1)	143.4(7)
C5–N1–N2	111.1(1)	112.4(7)	C15–N11–N12	111.4(1)	110.2(7)
N2–N1–C6	117.6(1)	117.6(7)	N12–N11–C16	117.5(1)	118.0(7)
C3–N2–N1	106.2(1)	105.8(7)	C13–N12–N11	106.4(1)	106.2(7)
N7–C6–N1	111.4(1)	110.0(8)	N17–C16–N11	110.8(1)	110.5(9)
O8–C6–N1	117.6(2)	117.6(8)	O18–C16–N11	117.9(2)	117.9(9)
C6–N7–Cu1	118.3(1)	119.2(6)	C16–N17–Cu1	119.4(1)	119.8(7)
N2–C3–C4	109.7(1)	108.6(8)	N12–C13–C14	109.4(1)	110.3(8)
N2–C3–C9	123.5(2)	121.6(8)	N12–C13–C19	122.2(2)	122.0(8)
N1–C5–C4	106.3(2)	104.3(8)	N11–C15–C14	106.1(1)	105.6(8)
N1–C5–C10	124.9(2)	121.1(8)	N11–C15–C20	124.6(2)	124.0(9)
C3–C4–C5	106.7(2)	108.9(9)	C13–C14–C15	106.8(2)	107.7(9)

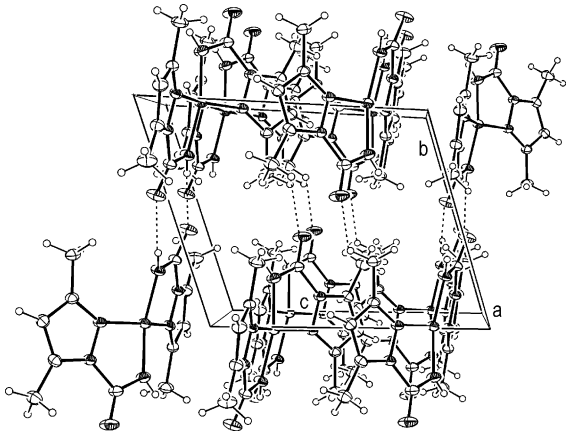

Fig. 5. Projections of the crystal packing along crystallographic '*a*' axis for Cu(L^3)$_2$.

3.2. Complex formation reactions

The influence of the anion on the complex formation was investigated using different copper(II) salts in conjunction with 1-carboxamide-3,5-dimethylpyrazole (HL^3) ligand. We have found that in the reaction of HL^3 with $CuBr_2$ a partial decarboxamidation of the ligand takes place, while with $Cu(OAc)_2$ no degradation was observed. In the latter case the Brønsted basicity of the acetate ion in methanol is high enough for the deprotonation of the ligand, replacing thus the voluminous acetate ion and yielding the **Cu(L^3)$_2$** complex. On the other hand, the complex formation with copper(II) chloride leads to a complete decarboxamidation of the ligand [26]. As the Brønsted basicity of both the chloride and bromide ions is too low for the deprotonation of the carboxamide group, the explanation of the complex formation with copper(II) bromide and chloride may be based on Pearson's theory [27–29], taking also into account the structural rearrangements and steric factors. In the presence of the hard chloride base a complete decarboxamidation of 1-carboxamide-3,5-dimethylpyrazole takes place, transforming the ligand to 3,5-dimethylpyrazole, which allows an intermediate hard–hard interaction between the copper(II) and the newly formed ligand. On the other hand, between the relatively small chloride ions and the ligand's methyl substituents the steric repulsion is weak. At the same time the elimination of isocyanic acid is probably promoted by ethanol, forming ethylcarbamate. With copper(II) bromide, decarboxamidation of the ligand occurs, too. However, only one ligand is transformed to 3,5-dimethylpyrazole, while the carboxamide group of the other ligand molecule is deprotonated, replacing thus one voluminous bromide ion. Two such molecules are

coupled through bromide bridges forming the dimeric **[CuBr(HL^1)(L^3)]$_2$** complex with mixed ligands.

3.3. Thermal decomposition of the compounds

The thermal decomposition of all the compounds was followed in an air and argon atmosphere with sample masses of about 5 mg. The thermal decomposition data in air are given in Table 5. As an example, the TG- and DTG-curves of the decomposition of **[CuBr(HL^1)(L^3)]$_2$** and **CuBr$_2$(HL^5)$_2$** in air and argon are presented in Fig. 6.

All the samples begin to decompose in the temperature range of 400–470 K. The lowest thermal stability exhibits the compound with the mixed 3,5-dimethylpyrazole and 1-carboxamide-3,5-dimethylpyrazole ligands, **[CuBr(HL^1)(L^3)]$_2$**, which in the context of the mixed soft–hard interaction can be understandable. The most stable complex is that with 5-amino-4-carboxamide-1-phenylpyrazole, **CuBr$_2$(L^2)$_2$**, presumably because of the $n \rightarrow \pi$ transition between the unshared electrons of the pyrazole nitrogen and phenyl nucleus.

The decomposition of **Cu(L^3)$_2$** in air results in an unstable intermediate around 470 K. In the mass spectrum recorded at the beginning of the decomposition, the molecular peak of 3,5-dimethylpyrazole, accompanied by the peaks of its fragments, was observed. This was followed by the peak of H_2 evolution. The intermediate was isolated and investigated by IR spectrometry. The characteristic changes in the IR spectrum include the disappearance of the ν(NH) vibrational band at 3302 cm^{-1} and the rise of new bands at 2241 and 2170 cm^{-1}. These latter bands can be assigned to coupled stretching vibrations of two isocyanate groups within a molecule. Another characteristic new band appears at 3122 cm^{-1} assigned to =CH$_2$ stretching vibrations. The spectrum contains additionally the bands of the methylpyrazole ligand, too. This is the consequence of the low stability of the intermediate, viz., the decomposition of the starting compound was

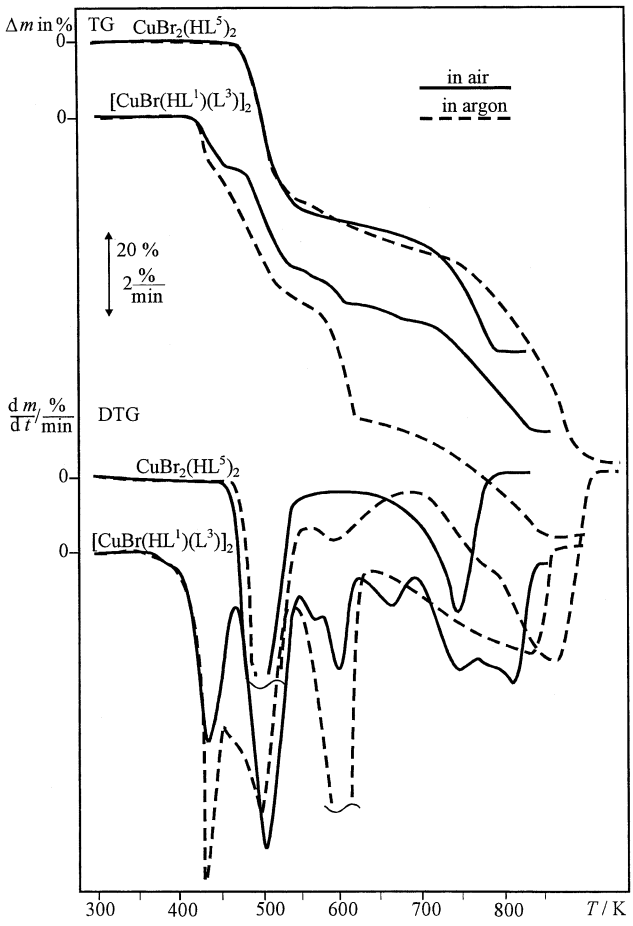

Fig. 6. TG-DTG curves for the CuBr$_2$(HL^5)$_2$ and [CuBr(HL^1)L^3]$_2$ in air and in argon.

Table 5
Thermal decomposition data in air

Compound	Temperature Range in K	Mass loss in %		Temperature in K	Residue (%)	
		Found (departing group)	Calc.		Found	Calc.
[CuBr(HL^1)(L^3)]$_2$	400–467	12.6 (-3,5-DMP)	12.72	830 CuO+CuBr	29.3 (1:1)	29.52
CuBr$_2$(L^2)$_2$	470–680	26.7 (-2Ph)	24.57	920 ?	27.5	
Cu(L^3)$_2$	425–485	30.0 ($-C_5H_{10}N_2$)	28.88	690 CuO	21.8	23.40
CuBr$_2$(HL^4)$_2$	430–530	8.0 ($-CH_3CO$)	8.57	930 CuO+CuBr	19.6 (1:1)	22.22
	530–725	14.5 (-5-MP-H)	15.97			
CuBr$_2$(HL^5)$_2$	465 –610	41.8 -2(3,5-DMP)	38.48	800 CuBr	27.0	28.71

3,5-DMP = 3,5-dimethylpyrazole; Ph = phenyl group; 5-MP–H = 5-methylpyrazole-H. The presence of the bromide in the end product was determined by a qualitative analysis.

not finished yet when the next decomposition step started. The elemental analysis (Found (%) C, 36.55; H, 3.7; N, 20.04, Required (%): C, 34.78; H. 2,50; N. 23,18) and mass loss data up to 500 K (Found (%) 30.0; Required (%): 28.88) as well as the IR results indicate an elimination process presented in Scheme 1. We note that an analogous isothiocyanate intermediate has been suggested for the formation mechanism of $[CuCl_2(HL^1)]_2$ and $CuCl_2(HL^1)_2$ complexes from 1-carboxamide-3,5-dimethylpyrazole [26].

The thermal decomposition of the pyrazole complexes is usually independent of purge gas up to 500–600 K. Above this temperature the degradation in argon slows down and in most cases is not finished up to 1100 K, as is the case with $\mathbf{CuBr_2(L^2)_2}$, $\mathbf{Cu(L^3)_2}$ and $\mathbf{CuBr_2(HL^4)_2}$ complexes. However, an interesting phenomenon was observed at the decomposition of the $\mathbf{[CuBr(HL^1)(L^3)]_2}$ and $\mathbf{CuBr_2(HL^5)_2}$ complexes: in argon above 900 K no residue was obtained. Unfortunately, at the end of the decomposition, by mass spectrometry we could not detect the evolved fragments, due to too high decomposition temperature. The different thermal decomposition pattern of the compounds in air and argon atmospheres may be explained by the increased basicity and acidity of the remaining components with increasing temperature [30]. Thus, in the $\mathbf{CuBr_2(HL^5)_2}$ and $\mathbf{[CuBr(HL^1)(L^3)]_2}$ complexes the covalency of the bonds is strengthened to the extent which allows a complete evaporation of the remaining parts of the molecule in argon.

The decomposition of the compounds starts with an endothermic reaction which is usually accompanied by the melting of the sample. The next step is an exothermic process except for $\mathbf{CuBr_2(HL^5)_2}$ and $\mathbf{[CuBr(HL^1)(L^3)]_2}$ complexes which is in agreement with the different thermal behavior of these compounds in argon.

4. Supplementary material

A full list of crystal data and refinement have been deposited at the Cambridge Crystallographic Data Centre, CCDC Nos. 179602 and 179603 for $\mathbf{Cu(L^3)_2}$ and $\mathbf{[CuBr(HL^1)(L^3)]_2}$, respectively. Copies of this information may be obtained free of charge from The Director, CCDC, 12 Union Road, Cambridge, CB2 1EZ, UK (fax: +44-1223-336-033; e-mail: deposit@ccdc.cam.ac.uk or www: http://www.ccdc.cam.ac.uk).

Acknowledgements

The authors (K. Mészáros Szécsényi) would like to thank the Domus Hungarica Scientiarum Artiumque Foundation for their support and the Hungarian National Scientific Research Foundation (OTKA, T-038189, A. Kovács). The work was financed in part by the Ministry for Science and Technology of the Republic of Serbia.

References

[1] S.R. Lukić, V.M. Leovac, A.F. Petrović, S.J. Skuban, V.I. Češljević, M.M Garić, Synth. React. Inorg. Met.–Org. Chem. 32 (2002) 873.
[2] (a) W.G. Haanstra, Ph.D. Thesis, Leiden University, Leiden, The Netherlands, 1991;
(b) W.G. Haanstra, W.A.J.W. van der Donk, W.L. Driessen, J. Reedijk, J.S. Wood, M.G.B. Drew, J. Chem. Soc., Dalton (1990) 3123.
[3] S. Trofimenko, in: S.J. Lippard (Ed.), Progress in Inorganic Chemistry, vol. 34, Wiley, New York, 1986, p. 115.
[4] N.T. Sorrel, Tetrahedron 45 (1989) 3.
[5] S. Trofimenko, Chem. Rev. 93 (1993) 943.
[6] R. Mukherjee, Coord. Chem. Rev. 203 (2000) 151.
[7] K. Mészáros Szécsényi, E.Z. Ivegeš, V.M. Leovac, L.S. Vojinovic, A. Kovács, G. Pokol, J. Madarász, Ž.K. Jacimovic, Thermochim. Acta 316 (1998) 79.
[8] K. Mészáros Szécsényi, E.Z. Ivegeš, V.M. Leovac, A. Kovács, G. Pokol, Ž.K Jaćimović, J. Therm. Anal. Cal. 56 (1999) 493.
[9] K. Mészáros Szécsényi, V.M. Leovac, Z.K. Jacimovic, V.I. Češljevic, A. Kovács, G. Pokol, J. Therm. Anal. Cal. 63 (2001) 723.
[10] A. Hergold-Brundić, B. Kaitner, B. Kamenar, V.M. Leovac, E.Z. Ivegeš, N. Juranić, Inorg. Chim. Acta 188 (1991) 151.
[11] M.N. Burnett, C.K. Johnson, ORTEPIII, Report ORNL-6895. Oak Ridge National Laboratory, Oak Ridge, TN, 1996.
[12] A. Szabó, V.I. Češljević, A. Kovács, Chem. Phys. 270 (2001) 67.

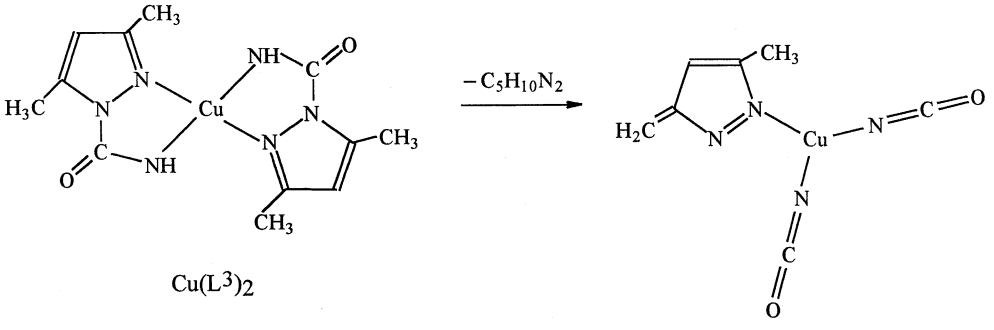

Scheme 1.

[13] G. Socrates, Infrared Characteristic Group Frequencies. Tables and Charts, 2nd ed., Wiley, New York, 1994.
[14] K. Nakamoto, Infrared and Raman Spectra of Inorganic and Coordination Compounds, in: Applications in Co-ordination, Organometallic and Bioinorganic Chemistry, Part B, 5th ed., Wiley, New York, 1997.
[15] Enraf-Nonius. CAD-4 Software. Version 5. Enraf-Nonius, Delft, The Netherlands, 1989.
[16] C.K. Fair, MolEN, An Interactive Intelligent System for Crystal Structure Analysis, Enraf-Nonius, Delft, The Netherlands, 1990.
[17] A.C. North, D.C. Philips, F. Mathews, Acta Crystallogr., A 24 (1968) 350.
[18] (a) A.L. Spek, Acta Crystallogr., A 46 (1990) C34;
(b) A.L. Spek, PLATON, A Multipurpose Crystallographic Tool, Utrecht University, Utrecht, The Netherlands,, 1998.
[19] G.M. Sheldrick, SHELXS86, Program for the Solution of Crystal Structures, University of Göttingen, Göttingen, Germany, 1985.
[20] G.M. Sheldrick, SHELXL97, Program for the Refinement of Crystal Structures, University of Göttingen, Göttingen, Germany, 1997.
[21] W.J. Geary, Coord. Chem. Rev. 7 (1971) 81.
[22] F. Valach, J. Kohout, M. Dunaj-Jurco, M. Hvastijová, J. Gazo, J. Chem. Soc., Dalton (1979) 1867.
[23] J. Gazo, I.B. Bersuker, J. Garaj, M. Kabesová, J. Kohout, H. Langfelderová, M. Melnik, M. Serátor, F. Valach, Coord. Chem. Rev. 19 (1976) 253.
[24] A.B. Neinding, Magnetochemistry of Transition Metal Complexes, Results in Sciences (Series Chemistry), Moscow (1970) 205 (in Russian).
[25] Z.K. Jacimovic, Ph.D. Thesis, University of Novi Sad, Faculty of Sciences and Mathematics, Yugoslavia (1998) 76.
[26] K. Mészárosszécsényi, Z.K. Jacimovic, V.M. Leovac, V.I. Češljevic, A. Kovács, G. Pokol, J. Therm. Anal. Cal. 66 (2001) 573.
[27] R.G. Pearson, J. Am. Chem. Soc. 85 (1963) 3533.
[28] R.G. Pearson, Science 151 (1966) 172.
[29] R.G. Pearson, J. Songstad, J. Am. Chem. Soc. 89 (1967) 1827.
[30] (a) L. Erdey, Period Politech Chem. 1 (1957) 91;
(b) L. Erdey, S. Gal, Talanta 10 (1963) 23.